South Eastern Australian Climate initiative

Final report for **Project 1.1.1P**

Relationship between the Hadley Circulation and the position and intensity of the sub-tropical ridge in the Australian region

Principal Investigator:

Dr. Bertrand Timbal, Centre for Australian Weather and Climate Research (CAWCR)
b.timbal@bom.gov.au,

and

Dr. Ian Smith, Centre for Australian Weather and Climate Research (CAWCR)
Ian.Smith@csiro.au

CSIRO Land and Water
Ph: 02 6246 5617
seaci@csiro.au
http://www.seaci.org

Australian Government
Department of Climate Change
Bureau of Meteorology

MURRAY–DARLING BASIN AUTHORITY

State Government Victoria Department of Sustainability and Environment

National Research FLAGSHIPS Water for a Healthy Country CSIRO

Project Abstract - Executive summary

Initial Project objectives:

- To assess the link between observed sub-tropical ridge (STR) trends and anthropogenic forcings.

Proposed methodology:

- Use the Drosdowsky (2005) methodology to diagnose trends in both the sub-tropical ridge intensity and position in several ensembles of climate model simulations of the 20th Century (CCSM run by NCAR, USA) forced with natural and anthropogenic forcings.

- Describe observed changes in the Hadley circulation using a theoretical model of the zonally averaged circulation

Summary of the findings:

The analysis of the CCSM3 simulations of the 20th Century shows that:

- The model has a realistic annual cycle of the STR intensity and position in the vicinity of Australia providing it is diagnosed using a broader longitude band than with the observations;

- The CCSM3 model produces an intensification of the STR at the end of the 20th Century only when anthropogenic forcing or both natural and anthropogenic forcings are used. Otherwise, there are no long-term trends in the simulations with natural forcing alone;

- The ensemble mean of the model forced with a combination of anthropogenic and natural external forcings provides the closest match of the three ensembles (natural, anthropogenic and full forcing) to the observations for both global warming (GW) and STR intensification;

- The relationship between these two variables (STR-I and GW) in the full forced ensemble shows strong similarities with the observed relationship, suggesting that what has been observed did not happen by chance; and

- In all simulations, the CCSM3 model exhibits lower than observed long-term trends in the STR (intensity or position) per degree of warming compared with the observations.

The theoretical modelling suggests that, if the tropical trends continue, then a continuation of the drying trends over southern Australia will continue. If the tropical trends are due to global warming, and this is primarily due to enhanced greenhouse gases in the atmosphere, then the theory provides a physical link between the enhanced greenhouse gases and the observed drying trends. This finding is therefore important in attributing the observed trends via climate model simulations. The main findings here are:

- The observed intensification and expansion of the tropics is consistent with an intensification of the descending branch of the Hadley Circulation (HC);

- This intensification for latitudes south of 30 °S is consistent with the drying trends that have been observed over southern Australia, including both the south-west of Western Australia and

the southern region of the Murray Darling Basin. It is also consistent with observed drying trends at similar latitudes in both hemispheres; and

- The intensification is also consistent with a weakening of the Walker Circulation and a tendency towards more "El Niño-like" conditions, as has also been observed.

Therefore, the theoretical modelling work lends considerable weight to the results of the attribution studies conducted under this project which utilize climate model simulations by providing a physical explanation between anthropogenic forcing and the observed drying trends in SEA through meridional circulation (HC) and STR intensification.

Acknowledgement:

This work was funded by the South Eastern Australia Climate Initiative. Thanks are due to the NCAR for making the CCSM3 outputs available and to Gary Strand and Julie Arblaster for providing the data.

Attachment A

Reproduction of the STR in 20th Century CCSM3 simulations

Dr Bertrand Timbal

Adapting the methodology to the CCSM3 simulations

The simulations used here with the Community Climate System Model version 3 (CCSM3) and performed by the NCAR (USA) are described in project 1.5.1 final report (Timbal et al., 2009) and in details in Collins et al. (2006). The model is run with well defined external forcings separated in three groups (Meehl et al., 2006):

1. anthropogenic - which includes greenhouse gases, aerosols and stratospheric ozone;
2. natural – which includes variations of the solar constant and volcanic eruptions; and
3. both natural and anthropogenic forcings combined (full forcings)

Each ensemble consists of five simulations with slightly different initial conditions (starting around 1850) enabling an estimation of the uncertainty of the climate signals. All 20th Century simulations were run until the end of 1999.

The ability of the CCSM3 to reproduce a realistic sub-tropical ridge (STR) in the vicinity of Australia was assessed using the methodology used by Drosdowsky (2005) to calculate observed STR position and intensity. One difference is that monthly values of observed mean sea level pressure (MSLP) used by Drosdowsky were on a 1 by 1 ° grid, while the CCSM3 has a resolution of 1.4 by 1.4 °. Monthly values of MSLP were first averaged for all the longitudes within a band from 145 to 150 °E (i.e. 4 longitudes for CCSM3). In order to provide a close match to Drosdowsky (2005), the location of the STR was defined as the latitude of the maximum pressure between 44 °S and 10 °S (42.7 °S and 10.5 °S in the case of the CCSM3); and the intensity of the STR was defined by the value of this maximum. Diagnosed this way, the annual cycle of the STR position and intensity in the CCSM3 model was relatively poor (Fig. 1); in particular the STR was diagnosed up to 4° too far north in spring. In order to provide a better reproduction of the annual cycle, the STR was subsequently diagnosed using a broader band of longitude (between 139.2 to 154.7 °E). Finally, two additional longitude bands were tried: one further east (green curve: 146.2 to 154.7 °E) and one further west (red curve: 137.8 to 149.1 °E). The best reproduction of the observed STR annual cycle was found with the latter (i.e. the further west) option.

All year around, monthly modelled values are, on average, within 0.8° and 0.9 hPa of the observed values. The intensity of the STR is too large from April to July (largest error is 1.2 hPa in June) and the position of the modelled STR is not as far south as observed (by about 1 to 1.2 °) in January and February. Overall, while keeping these errors in mind, the ability of the model to produce a STR similar in location, intensity and with the right annual cycle was found to be suitable, providing the STR is diagnosed on a broader longitude band than for the observations (Fig. 2). The larger band further west better encompasses the actual location of the observed maximum pressure during the peak of the STR intensity in May-June-July, which is centred on the Australian continent and it also overlaps better with the SEACI area of interest. It is also worth noting that the choice to use a narrow band along the eastern seaboard was driven in part by the availability and reliability of long climatic record of MSLP (Drosdowsky, pers. comm.).

Decadal STR trends in CCSM3 simulations

For each CCSM3 simulation, 11-year running means were computed for each of STR intensity, position and global average temperature. Anomalies, expressed relative to the century long climatology, are shown as a single average from the five members of each of the three ensembles and are compared with the observations in Fig. 3. Running means are used to remove most of the lower frequency variability (on inter-annual time scale) and to focus on the results at decadal and centennial time-scales. When full forcings (which are expected to provide the most realistic external forcings) are used, the model response is very similar to the observations. The model produces a global warming similar in magnitude to the observations (about 0.9 °C over the century compared to 0.8 °C for the global temperature dataset (Climatic Research Unit, University of East Anglia, UK, Brohan et al., 2006) and a strengthening of the STR which, as per the observations, appears to occur simultaneously. In both the observations and model simulations, epochs of warming alternate with periods of no significant warming. For example, warming occurs from around 1900 to the 1940s and from 1970 to now in the observations. This compares with warming from 1900 to the 1950s and from 1975 to now in the model. Similarly, the STR strengthening is not regular with time and appears to plateau at the times when no significant warming occurred (e.g. around the middle of last century). The confirmation of the covariance of the GW and STR build up in the CCSM3 simulations reinforced earlier suspicions that the observed relationship did not occur by chance, and is linked to some large-scale changes in the climate system dynamics and energetics, most likely involving the transfer of energy from the Equator to higher latitudes through meridional circulations (e.g. the Hadley Cell). The mechanics of these changes in circulation are further discussed in the theoretical modelling section.

The strengthening of the STR in the ensemble mean (about 0.6 hPa for the full forcings ensemble) is much reduced compared to the observed values (1.2 hPa). Note: the Y-axis scale for the STR intensity is on the left of the graph (the right Y-axis is for temperature) and, while the right scale is unchanged between graphs, the left scale is amplified by a factor 3 for model results compared to the observations. This result is consistent with earlier findings for MSLP changes in the northern hemisphere (Gillett et al., 2003) and is worth exploring further by looking at individual members of the full forcings ensemble (Fig. 4) to avoid the smoothing issue that arises when comparing an ensemble of simulations with a single realisation for the observations. Individual simulations exhibit much more dramatic rises and falls during the 20th Century, typically of the order 1 hPa over a 20 to 40 years period, which is comparable to observed rises of 1 hPa in the 1930s and 1940s and 0.8 hPa since the 1970s. However centennial trends for individual ensemble members are not much larger than for the ensemble mean and are always lower than the observed trend. It is also interesting to compare the temporal relationship between STR intensification and GW in each individual simulation. Although the match is not as close as with the ensemble mean, which is in part due to more abrupt decadal variability, there are several instances when the model simulations display concomitant periods of sustained warming and STR strengthening.

Besides the model ability to reproduce the relationship between observed STR intensification and GW, a second important finding from the model simulations of the 20th Century is the role of the various external forcings in simulating realistic changes. The ensemble of simulations with the CCSM3 model forced with natural forcings (solar variability and large volcano eruptions) alone (Fig.3 bottom left) does not exhibit either long-term warming or STR strengthening. In these simulations, there is a small warming (about 0.2 °C) up to the 1960s with cooling thereafter and no centennial trends. Similarly in the absence of strong global warming, the STR intensity exhibits sizeable decadal variability (changes of up to 0.5 hPa) but no long-term trends. On the contrary, simulations forced with anthropogenic forcings (greenhouse gases, aerosols and stratospheric ozone changes) alone (Fig. 3 bottom right) show a 0.7 °C global warming during the 20th Century which accelerates significantly in the last 20 years. In these simulations a strengthening of the STR in the latter part of the simulations (from the 1970s) is shown, again suggesting a response to

prolonged global warming. However, in the early part of the simulations a large decrease in STR intensity is observed until the 1930s, which does not show a relationship with the global temperature curve.

In addition to examining responses in terms of annual means, it is also worth further exploring relationships during May to October when the relationship between STR intensity and south-eastern Australia SEA rainfall is the strongest (Timbal et al., 2007). For this period, modelled STR intensity and location (Fig. 4 lower graphs) are compared with the observations using 21-year running means (Fig. 4 upper graphs). A longer smoothing filter is applied in this instance as the STR movements are noisier on a 6 monthly time period compared to annual means. The relationship between May to October STR intensity and global annual temperature is very strong in the observations as well as in the CCSM3 simulations. However, as noted earlier, the modelled strengthening is much smaller in magnitude compared to observed (0.6 hPa instead of 1.2 hPa). The latitudinal shift of the STR is noisy in the observations: there is a large shift south (upward on the graphs) between the 1920s and 1940s at a time of significant warming, but otherwise it appears as multi-decadal variability unrelated to the global temperature. The movements of the STR in the CCSM3 model are relatively small, but an on-going positive trend is visible (a shift southward of 0.5 ° in latitude).

Centennial STR trends in CCSM3 simulations as a function of global warming

The 15 individual simulations of the 20th Century with CCSM3 were used to further investigate the relationship between STR movement and GW. For all simulations, centennial linear trends were calculated for both GW and STR intensity and position (annual and May to October means were computed).

There is a strong relationship between GW and STR intensity and position (Fig. 6); correlations vary between a high of 0.73 (for annual STR position) and a low of 0.54 (for May to October STR position), and all correlations are statistically significant at the 95 per cent level.

The slope of the relationship between GW and STR intensity is 0.63 hPa per degree of warming for the STR in May to October but only 0.37 hPa for the annual mean (Fig 6, top panels). Shifts in latitude are less seasonal: 0.44 °S per degree of warming for the annual mean and 0.5 °S for the May to October period (Fig 6 bottom panels). Individual simulations are clustered according to the forcings used: almost no warming with is associated with natural forcings, a warming comparable to the observed is associated with anthropogenic forcings, and a slightly larger warming is associated with the full forcings. The associated STR response is also seen to be largest with the full forcings.

It is worth noting that the response computed by taking the ensemble means (shown by coloured squares on the graphs) of any ensemble is always very close to the line of best fit across all members. In all cases however, the observations (black point) stand out as showing a much larger response of the STR to GW: 1.5 hPa per degree of warming for the intensification (2.2 hPa in May to October) and a shift of 1.5 °S (2.6 °S in May–October). With only a single realisation for the observed climate system over the past century, it is not possible to rule out the possibility that these values are large by chance; however, it does suggest that the CCSM3 has a tendency to under-represent the response of mid-latitude MSLP around Australia. This is important as it drives the rainfall decline. This result sheds light on earlier findings during Phase 1 of SEACI (Project 1.5.1) where the direct model rainfall signal for SEA in the CCSM3 simulations with full forcings was relatively small (Timbal et al. 2009). Once CCSM3 was downscaled (using the Bureau of Meteorology Statistical Downscaling Model (SDM)), it was found that the rainfall decline was sizeable but still not as large as observed, particularly in autumn. The enhanced signal from the SDM, which nevertheless remains lower than observed rainfall decline, is due to MSLP being one of

the key predictors for the SDM which incorporates much of the STR strengthening signal diagnosed here. Results from Project 1.5.1 and this analysis are consistent in suggesting that the CCSM3 model forced with full forcings produces a climate change around SEA comparable to what has been observed (in terms of MSLP changes, STR strengthening and rainfall reduction) but with a lesser magnitude.

Conclusions

The relationship between global warming and STR was investigated using a 15 member ensemble of simulations of the 20th Century. Of these 15 members, equal numbers were forced with natural external forcings (e.g. solar variability and volcanoes) only, external anthropogenic forcings (e.g. greenhouse gases, aerosols and ozone) only, and a combination of both natural and anthropogenic forcings (i.e. full forcings). It was found that the observed relationship between the STR intensification and global warming (Timbal et al. 2007) when long-term smoothing is used (11-years running mean) is unlikely to have occurred by chance. Indeed, the fully forced ensemble displays a similar rise of temperature to that observed, and a strengthening of the STR which appears to mimic the time evolution of GW over the century. It is worth noting however, that in general the simulated strengthening of the STR is weaker than observed, and the match between GW and the STR build up is not as strong in individual simulations. It is very clear that the naturally forced ensemble does not display any sizeable GW trend nor STR intensification.

Attachment B

Theoretical modelling of the Hadley Circulation

Ian Smith

Introduction

A shift to drier conditions over recent decades has resulted in serious reductions to inflows to rivers and dams in both the south-west of Western Australia and the Murray Darling Basin system of south-east Australia. Research conducted under the SEACI and IOCI programs has provided insights into the nature of these drying trends and has highlighted the importance of shifts in the large scale atmospheric circulation. At the same time, northern Australia is experiencing a trend towards wetter conditions while there has been a well-documented shift towards more El Niño–Southern Oscillation (ENSO) -like conditions over the tropical Indo-Pacific region.

It is quite possible that all these changes are linked but there is presently no framework for addressing this other than to resort to the results of global climate models. The absence of any such framework, and the total reliance on the output of climate models, is not satisfactory – particularly when attempting to provide more reliable and less uncertain projections of future climate change. On the other hand, our understanding of the basic features of the zonally averaged circulation is not sufficient to provide satisfactory answers to this problem. For example, the Hadley Circulation (HC), which represents large scale overturning of the atmosphere for over half the globe, is described as a thermally direct circulation – driven by the requirement to export excess heat from the warm equatorial regions to the cooler high latitudes. Theories which attempt to describe its key features often refer to factors such as gradients in surface temperature, latent heat release from convection and heat fluxes. The Ferrel Circulation (FC), which is a relatively smaller companion overturning circulation pattern at higher latitudes, is often described as an indirect circulation.

Despite a number of theoretical studies, our understanding of the zonally averaged circulation does not provide simple answers to questions such as: Why do the trade winds blow from east to west? What determines the strength and intensity of the HC? What is the link between mid-latitude westerlies and the trade winds? What determines the strength and extent of the FC? What is the nature of the link (if any) between the HC and the FC? What is the link between the trade winds, mid-latitude westerlies, and polar easterlies? Why is there a difference between the Northern and Southern Hemisphere winds? Can we explain the apparent link between ENSO events and the HC?
For example, Webster (2002) summarizes much of the current state of knowledge about the HC and, although the basic elements are identified, it is apparent that there are no simple explanations. The FC is described as "…. merely a by-product of the very strong poleward transport of energy by the waves in the westerlies", while the location of the Inter-Tropical Convergence Zone (ITCZ), the influence of sea surface temperatures (SST), cross-equatorial pressure gradients, convection, moist thermodynamics, the vertical transport of heat at the equator and monsoons are all cited as important components of the HC. He concludes that "...physical explanations of the Hadley circulation are rather complicated."

Here we make an attempt to provide a framework where these questions can be partly addressed. We propose that the key to the problem is the requirement that the large scale circulation satisfies the continuity equation on a sphere, the important dynamic terms involve just the Coriolis force, surface friction and a constant representing the divergent flux of eddy momentum – the latter being determined by the requirement to maintain conservation of angular momentum. It is shown how a simple 2-level model approach to the problem yields relatively simple mathematical solutions for

the zonally averaged quantities U, V and W. It is shown how these solutions provide a basis for better understanding the questions above and, in particular, provide an explanation for the following observed trends: enhanced tropical precipitation, weaker trade winds, mid-latitude drying and poleward shifts in the mid-latitude storm tracks.

2-level model solutions for W and V

We assume a simple 2-level model of the zonally averaged circulation (Figure 7). V_L (a function of latitude φ) represents the zonally averaged meridional wind within the lower level, while V_U represents its counterpart within the upper level. Assuming no vertical flow at the surface, nor at the top of the atmosphere *Z, W* (also a function of φ) represents the zonally average vertical wind at the interface between the two levels. As drawn, the Southern Hemisphere meridional circulation comprises a Hadley cell operating at low to mid-latitudes, but an undetermined circulation pattern at higher latitudes. This reflects the fact that W and V, being relatively small in comparison to U, are difficult to measure and the details of their structure are unclear at these latitudes.

In this 2-level model, the equation of continuity under steady state conditions, and assuming constant density is:

$$V_L \cos\phi = -V_U \cos\phi \approx \int W(\phi) \cos\phi \, \partial\phi \quad (1)$$

Where ~ denotes the fact that the solution describes the shape and not the absolute values. This expresses the fact that the mass transport (northwards) at the lower level is balanced by mass transport (southwards) at the upper level and, that at any latitude, the amount being transported is equal to the integrated mass transport across the interface.

Any solution to this equation must satisfy $V_L = V_U = 0$ *at* $\varphi = -90$ *and* $\varphi = 0$. i.e. there is no net transport beyond the pole nor the equator. This imposes some constraints on the function $W(\varphi)$. A simple function such as:

$$W_N(\phi) = w_N \cos N\phi$$

Where w_N is a constant and N (>1) is odd satisfies these constraints. We are interested in the two simple functions W_3 *and* W_5 which yield the following solutions for the meridional velocity:

$$V_3 \approx \frac{1}{\cos(\phi)} \int \cos(\phi)\cos(3\phi)\,\partial\phi \approx \frac{1}{\cos(\phi)} \left[\sin(2\phi)/2 + \sin(4\phi)/4 \right] \quad (2)$$

and

$$V_5 \approx \frac{1}{\cos(\phi)} \int \cos(\phi)\cos(5\phi)\,\partial\phi \approx \frac{1}{\cos(\phi)} \left[\sin(4\phi)/4 + \sin(6\phi)/6 \right] \quad (3)$$

The scaling factor which determines the magnitude of the solutions is: $\frac{Rw_N}{Z}$

Where *R* is the radius of the Earth, *Z* is the depth of the atmosphere and w_N is the magnitude of the corresponding vertical velocity function.

Figure 8 shows the two trigonometric functions W_3 and W_5 while Figure 9 shows the corresponding solutions V_3 and V_5. In the first case, W_3 has maximum values at $\varphi = -60$ *and* $\varphi = 0$ and V_3 is characterized by positive values at all latitudes, with a maximum φ= -30. In the second case, W_5 has maximum values at $\varphi = -72$, $\varphi = -36$ *and* $\varphi = 0$, while V_5 is characterized by negative values between the pole and $\varphi = -38$, and positive values between this latitude and the equator.

W_3 is a plausible representation of the vertical velocity field, since it is consistent with the concept of a heating in the tropics (ascending motion) and a cooling source at higher latitudes (descending motion) as implied in Figure 7. However, the resulting solution V_3 is not plausible since it comprises positive values at all latitudes which imply easterly zonal winds at all latitudes as a consequence of deflection by the Coriolis force. i.e. a single cell circulation is unrealistic. W_5, on the other hand, appears at first glance to be unrealistic, since it implies vertical motion at the high latitudes, similar in magnitude as that at low latitudes. However, the resulting solution V_5 is very plausible since it implies convergence at the pole and equator, balanced by divergence at mid latitudes. The fact that V_5 changes sign implies more than one circulation cell.

There are an infinite number of solutions for W and V but, as will be shown, these two are sufficient to lead to quite plausible solutions for the low-level zonal wind (U).

Two-level model solutions for U

The equation of motion for the zonal wind (*u)* on a rotating Earth is:

$$\frac{\partial u}{\partial t}+u\frac{\partial u}{\partial x}+v\frac{\partial u}{\partial y}+w\frac{\partial u}{\partial z}-\frac{uv\tan\phi}{R}+\frac{uw}{R}=-\frac{\partial p}{\rho\partial x}+2\Omega v\sin\phi-2\Omega w\cos\phi+F_x$$

where p represents the local pressure and F_x represents surface friction (c.f. Peixoto and Oort, 1992, Equn. 3.9a).

Assuming steady state conditions ($\partial / \partial t = 0$), ignoring terms involving *1/R and w* (assumed small in comparison to other terms), and taking zonal averages within the lower level (when the pressure gradient term $\partial p/\partial x$ disappears) leads to the following expression (Equn, 13 in Cook, 2004):

$$0=-\frac{\overline{\partial uv}}{\partial y}+fV_L-F_x$$

which expresses a balance between the average meridional (negative divergence) /convergence of momentum flux, the average Coriolis force and the average surface frictional force. Letting G represent the divergent momentum flux, assuming a Newtonian approximation for the last term (a product of U and a friction coefficient K) and rearranging yields:

$$KU_L=fV_L-G$$

Assuming V is known, this only yields a solution for U if the momentum flux term (G) can be parameterized. We first invoke the simple constraint that the area weighted surface shear stress over the entire globe must sum to zero under steady state conditions. i.e. there can be no net zonal torque. This requires:

$$\int_{-90}^{90}KU_L\,\partial\varphi=\int_{-90}^{90}(fV_L-G)\,\partial\varphi=0$$

The simplest parameterization is to assume G is a constant (G*). A solution for U_L is then given explicitly by:

$$KU_L=fV_L-G^*\quad,\quad G^*=\int_{-90}^{90}fV_L\partial\varphi \qquad (4)$$

Substituting V_3 *and* V_5 leads to the following simple solutions:

$$U_3 \approx \tan(\phi)\left[\sin(2\phi)/2 + \sin(4\phi)/4\right] + 1.1 \quad (5)$$

and

$$U_5 \approx \tan(\phi)\left[\sin(4\phi)/4 + \sin(6\phi)/6\right] + 0.01 \quad (6)$$

In each case the numerical value represents -G* which, being positive, implies westerly winds at the equator (θ= 0).

The scaling factor which gathers up the various constants is represented by: $\frac{2\Omega R w_N}{KZ}$

i.e. the magnitude of the zonally averaged wind increases with the rotation rate Ω, Earth's radius *R*, the magnitude of the vertical velocity *w*. It decreases with the magnitude of the frictional constant *K* and with depth of the atmosphere *Z*.

Figure 10 shows the resulting functions U_3 and U_5. As expected, U_3 is not a plausible solution since it corresponds to westerlies in the tropics and high latitudes, and easterlies at mid-latitudes. On the other hand, although U_5 is far more plausible, it is also characterized by slightly westerly winds at the equator.

Since neither solution on its own is satisfactory, we investigate solutions based on a linear combination of the two functions W_3 and W_5:

$W(S) = W_5 (\cos(5\varphi) + S \cos(3\varphi))$ (7)

where *S*, a shape factor, represents the relative strength of W_3 relative to W_5. i.e. for *S=0* the function reverts to W_5, for *S* large the function is dominated by W_3.

The interesting solution for *U* is that based on a value for *S* of -0.6. This is shown in Figure 11a compared to observed, annual, low level (1000hPa) zonally averaged winds based on reanalysis data. The solution for *U* has been scaled for comparison with the observations. The key features of this solution include the close similarity with the observed winds from about *-70° to +30°*. The westerly wind maximum is in the correct location, as is the point where the westerlies transform to easterly trade winds in the tropics. The relative strength of the westerlies and easterlies is well captured. The solution also includes a minimum in the trade wind strength at the equator. Beyond +30°, the solution overestimates the strength of the westerlies and implies significant polar easterlies in the northern hemisphere. While these differences with the observations appear significant, they can largely be overcome by recognizing that frictional effects in the northern hemisphere will be much larger than those in the southern hemisphere because of the different distributions of land, ocean and mountains. i.e. a better match can easily be obtained by increasing the constant K applicable to the northern hemisphere. It appears as if an increase by about a factor of 3 would be required to provide a closer match with the observations. Note that a different value for K in either hemisphere does not alter the fundamental solutions.

Variations to the solution for U

In this section we consider how variations in the parameter S (which controls the relative influence of the functions W3 and W5) affect the solutions for V and U.

Figure 12a shows the effect of varying S (between 0 and -0.8) on the various solutions for W, V and U. It can be seen that as S varies from 0 to -0.8, the nature of the solutions changes systematically. In Table 1, changes in key features of the solutions as S goes from -0.8 to 0.0 are summarized. It is worthwhile noting that many of the implied changes listed in Table 1 have been indicated by several observational studies of recent decades.

Discussion and Conclusions

The model described here is based on minimal assumptions. We assume a 2-level representation of the global atmosphere, constant density, steady-state conditions, a scaled version of the equation of motion (for zonal average U) and a Newtonian expression for surface friction. The key assumption is that the meridional momentum flux gradient is constant, but determined by the requirement that the net surface shear stress over the globe sums to zero. In effect, this term represents a counterweight to the shear stresses induced by the Coriolis term (*fV*). The other assumption, although not necessary, is that the zonal average vertical velocity function (for Earth at least) is represented by a linear combination of the first two permissible cosine functions. An optimal combination (S=-0.6) provides a realistic simulation of present day large scale features – particularly in the SH.

As a consequence, we can derive expressions for the low level W,V and U which indicate of the strength, location of the Hadley and Ferrel Circulations, the strength of the equatorial (trade) winds and the mid-latitude westerlies, and the location of regions of ascent/descent which should correspond to the locations of relatively high/low rainfall. These agree surprisingly well with observations, more so since the model makes no direct reference to pressure gradients, topography, atmospheric stability, temperature/heat fluxes, humidity/water vapour fluxes, geostrophy, jet streams, nor the stratosphere. These features distinguish it from most other explanations of the zonal average circulation, particularly theories which attempt to describe the strength and location of the Hadley Circulation.

Apart from being easily testable, the model provides the following insights about how the large scale global circulation can adjust:

1. As the vertical velocity increases (from the equator to +-30^{o}) it simultaneously decreases in the extra-tropics but then increases at higher latitudes (Figure 6a);

2. The zone of equatorward flowing meridional winds increases at low latitudes, while the zone of poleward flowing meridional winds decreases at higher latitudes (Figure 6b);

3. The trade winds decrease equatorward of +-20^{o}, yet the zone of easterlies expands south of this latitude. Furthermore, the strength of the mid-latitude westerlies decreases (Figure 6c).

The conclusions arising from the theoretical modelling were listed in the executive summary. It provides an important explanation for other SEACI findings on the relationship between anthropogenic forcings and observed drying trends in south-eastern Australia.

References:

Allan, R. and Ansell, T., 2006: A newly globally complete monthly historical gridded mean sea level pressure dataset (HadSLP2): 1850-2004, *J Climate*, **19**, 5816–5842

Allan, R. P., and B. J. Soden, 2007: Large discrepancy between observed and simulated precipitation trends in the ascending and descending branches of the tropical circulation. *Geophys. Res. Lett.*, **34**, L18705, doi:10.1029/2007GL031460

Brohan, P., J.J. Kennedy, I. Haris, S.F.B. Tett and P.D. Jones, 2006: Uncertainty estimates in regional and global observed temperature changes: a new dataset from 1850. *J. Geo. Res.,* **111**, D12106, doi:10.1029/2005JD006548

Collins, W. D., and Co-authors, 2006: The Community Climate System Model version 3 (CCSM3). J. Climate, **19,** 2122–2143

Cook (2004) Hadley Circulation dynamics: Seasonality and the role of continents, In: *The Hadley Circulation: Present, Past and Future,* Diaz, Henry F.; Bradley, Raymond S. (Eds.), Kluwer Academic Publishers, 511pp

Drosdowsky, W., 2005: The latitude of the subtropical ridge over eastern Australia: the L index revisited. *Int J of Clim*, **25**, 1291-1299

Frierson, D., J. Lu and G. Chen, 2007: The width of the Hadley cell in simple and comprehensive general circulation models*. Geophys. Res. Lett*. 34, L18804.

Gillette, N.P, F.W. Zwiers, A.J. Weaver and P.A. Stott, 2003: Detection of human influence on sea-level pressure, *Nature*, **422**, 292-294

Hu, Y. and Fu, Q (2007) Observed poleward expansion of the Hadley circulation since 1979. *Atmos. Chem. Phys*. 7, 5229–5236

Lu, J., Vecchi, G. A. and T. Reichler (2007): Expansion of the Hadley cell under global warming. *Geophys. Res. Lett.* 34, L06805

Meehl, G. A., W. M. Washington, B. D. Santer, W. D. Collins, J. M. Arblaster, A. Hu, D. Lawrence, H. Teng, L. E. Buja, and W. G. Strand, 2006: Climate change projections for twenty-first century and climate change commitment in the CCSM3, J. Clim., **19**, 2597– 2616

Peixoto, J.P and A.H. Oort (1992) Physics of Climate. Melville, New York: American Institute of Physics, 520 pp

Power, S. B. and I.N. Smith, 2007: Weakening of the Walker Circulation and apparent dominance of El Niño both reach record levels – but has ENSO really changed? *Geophys. Res. Lett*., 34, L18702, doi:10.1029/2007GL030854

Seidel, D. J. and R.J. Randel, 2007: Recent widening of the tropical belt: Evidence from tropopause observations. *J. Geophys. Res*., **112**, D20113

Timbal, B., B. Murphy, K. Braganza, H. Hendon, M. Wheeler and C. Rakich, 2007: "Compare documented climate changes with those attributable to specific causes". South-Eastern Australian Climate Initiative (SEACI), final report for project 1.1.2, 19 pp

Timbal, B., E. Fernandez and J. Arblaster, 2009: "Application of the Bureau of Meteorology downscaling technique to coupled climate model simulation of the 20th Century and implications of the attribution of observed climate change", South-Eastern Australian Climate Initiative (SEACI), final report for project 1.5.1, 25 pp

Vecchi, G. A., A. T. Wittenberg, I. M. Held, A. Leetmaa, and M. J. Harrison, 2005: Weakening of tropical Pacific atmospheric circulation due to anthropogenic forcing. *Nature*, **441***,* 73–76
Webster, P., 2004: The elementary Hadley Circulation, In: The Hadley Circulation: Present, Past and Future, Diaz, Henry F.; Bradley, Raymond S. (Eds.), Kluwer Academic Publishers, 511pp

Appendix: Tables and figures

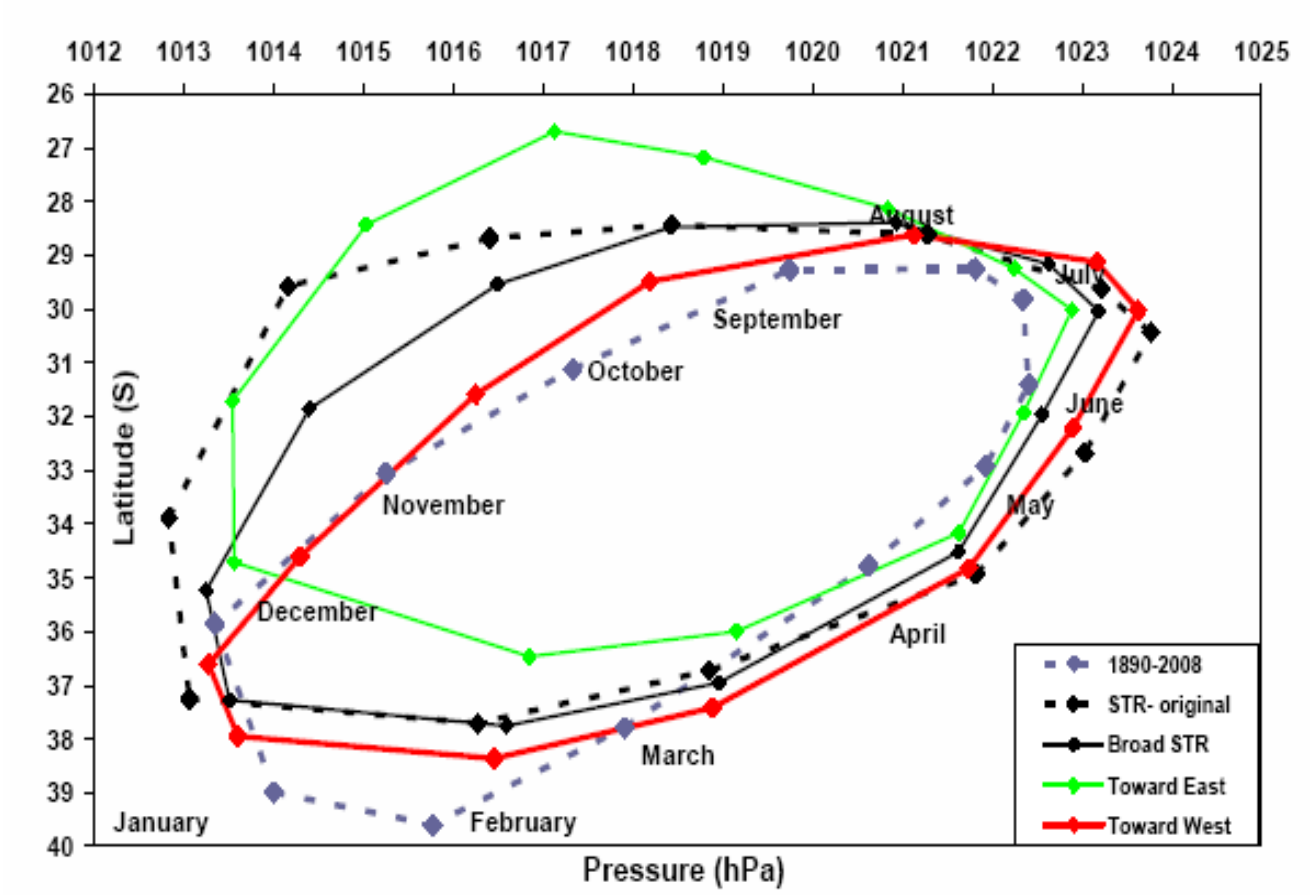

Fig. 1: *Annual cycle of the sub-tropical ridge intensity and position from the observations (dashed grey line) and diagnosed from a CCSM3 simulation of the 20th Century using different longitude bands (see text for details)*

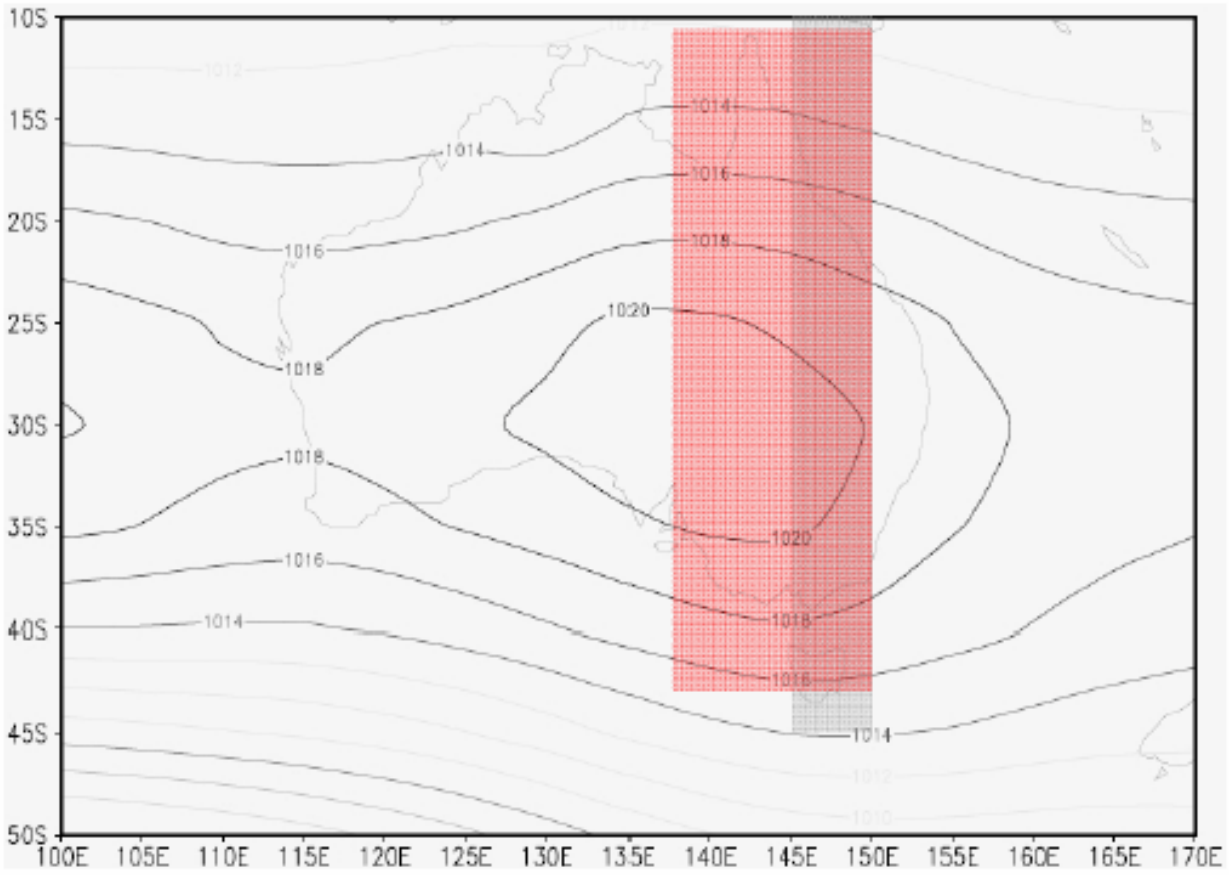

Fig. 2: *Geographical area used to diagnose the STR in the observations (grey band) and in the CCSM3 simulations (red band) overlaid above the long-term 1850 to 2004 mean of MJJ MSLP from the HadSLP2 dataset around the Australian continent.*

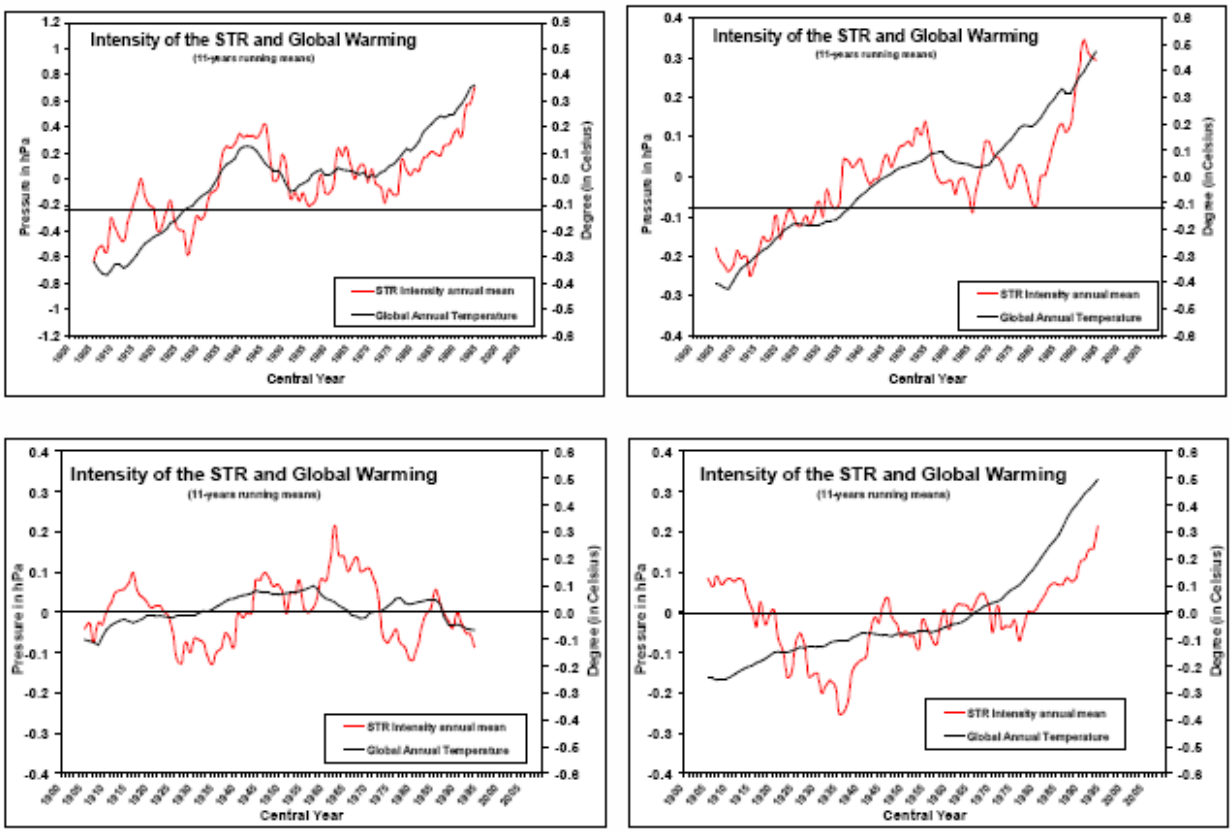

Fig. 3: *11-year running means of anomalies of annual STR intensity (in hPa on the left Y-axis) and global temperature (in °C on the right Y-axis) calculated from the century long climatology for the observations (top left), the ensemble of CCSM3 simulations with full forcings (top right), natural external forcings only (bottom left) and anthropogenic external forcings only (bottom right).*

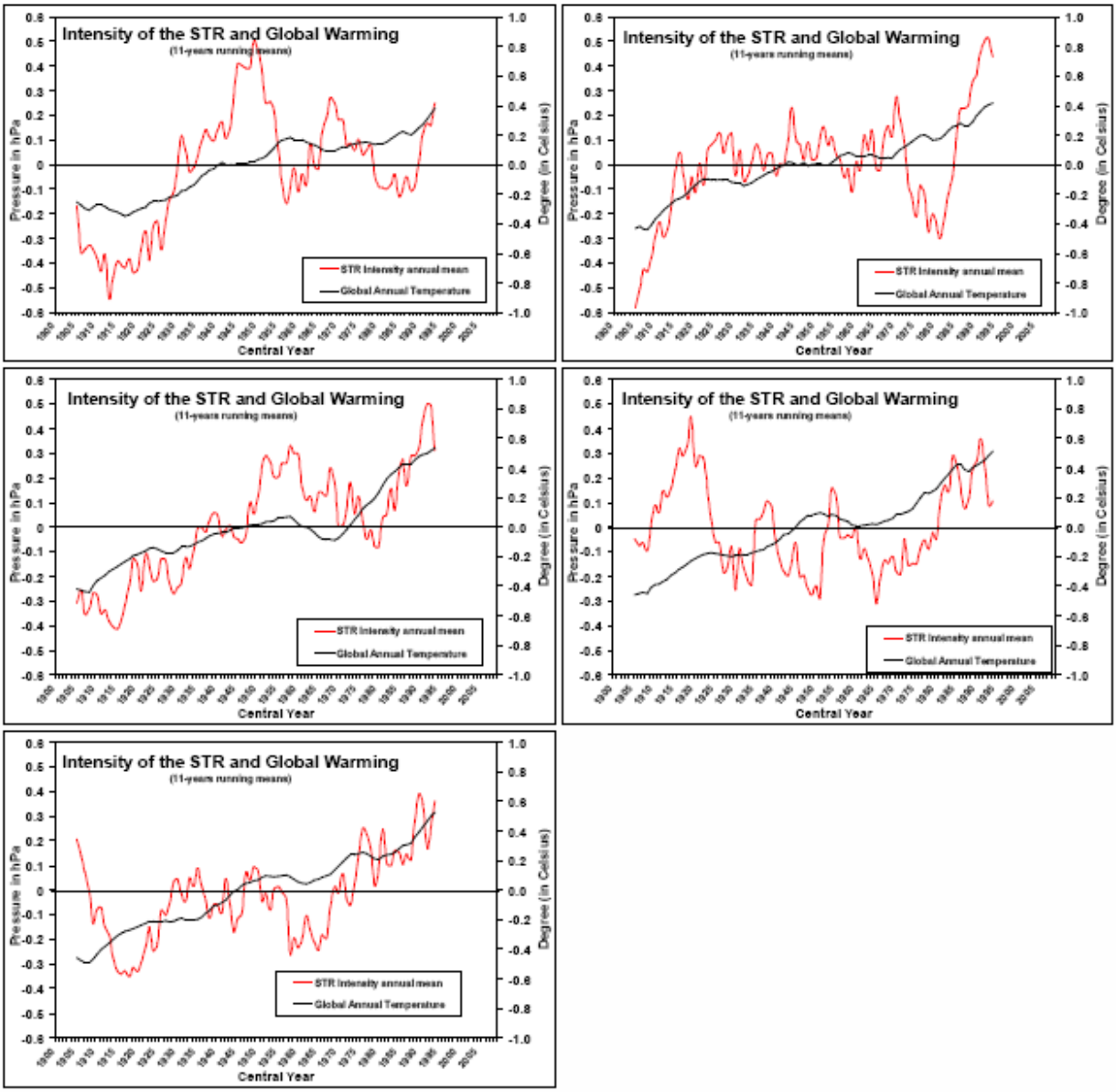

Fig. 4: *As per Fig. 3 but for the five individual simulations forced with full forcings (Note: both Y-axis scales differ from Fig. 3).*

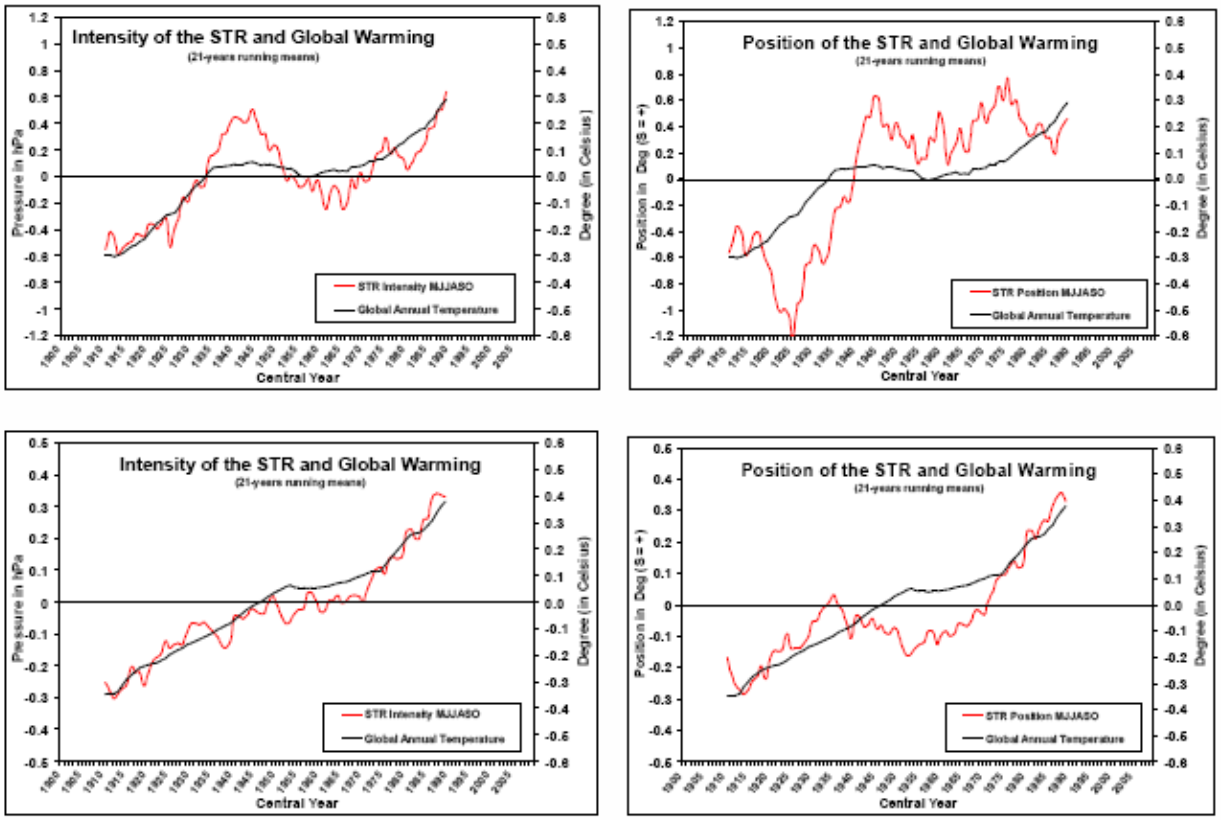

Fig. 5: *21-year running mean of anomalies of STR intensity (left) and position (right) in May-June-July-August-September-October compared with global warming for the observations (top row) and the CCSM3 ensemble forced with full forcings (bottom row).*

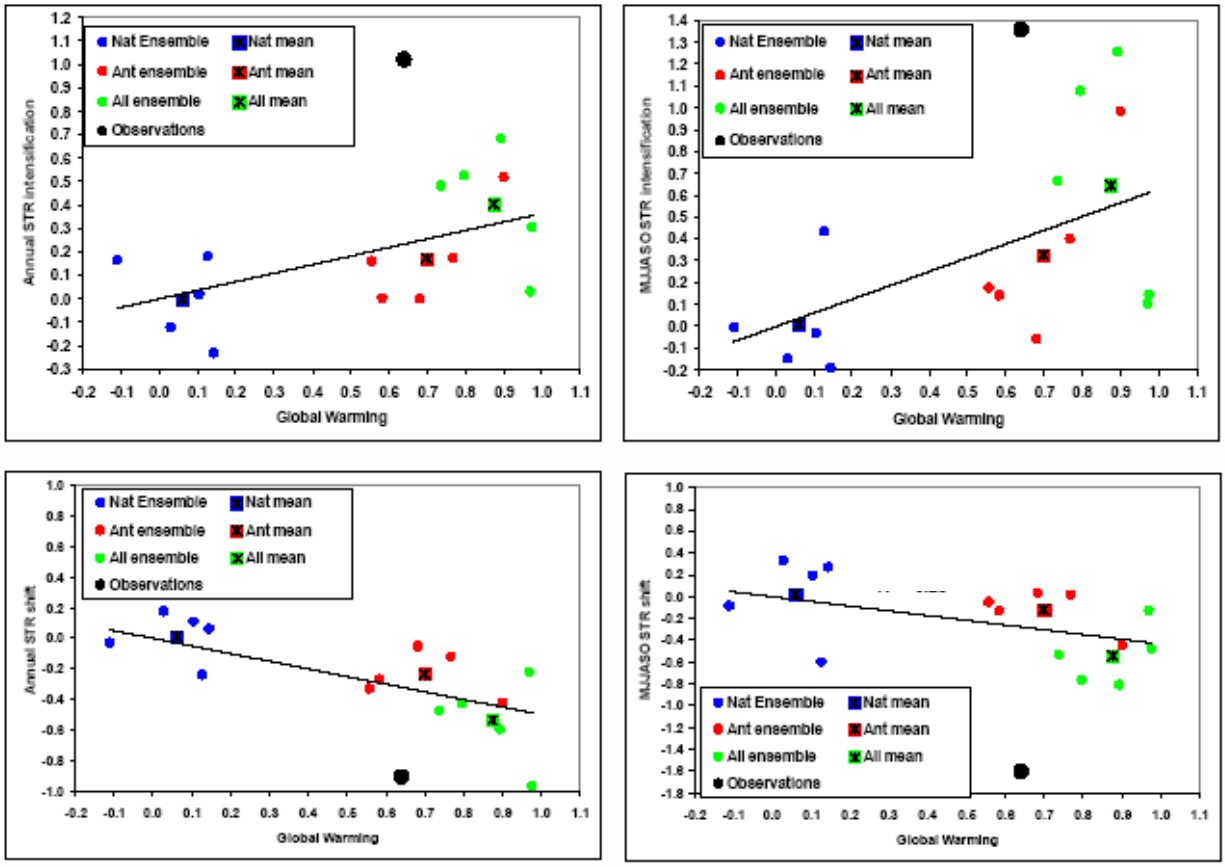

Fig. 6: *Centennial linear trend for each of the 15 CCSM3 simulations of the 20th Century for STR intensity (upper) and position (lower) annual mean (left), and May to October mean (right) as a function of the modelled global warming; ensemble means are shown as well as the observations. The lines of best fit to the results are shown.*

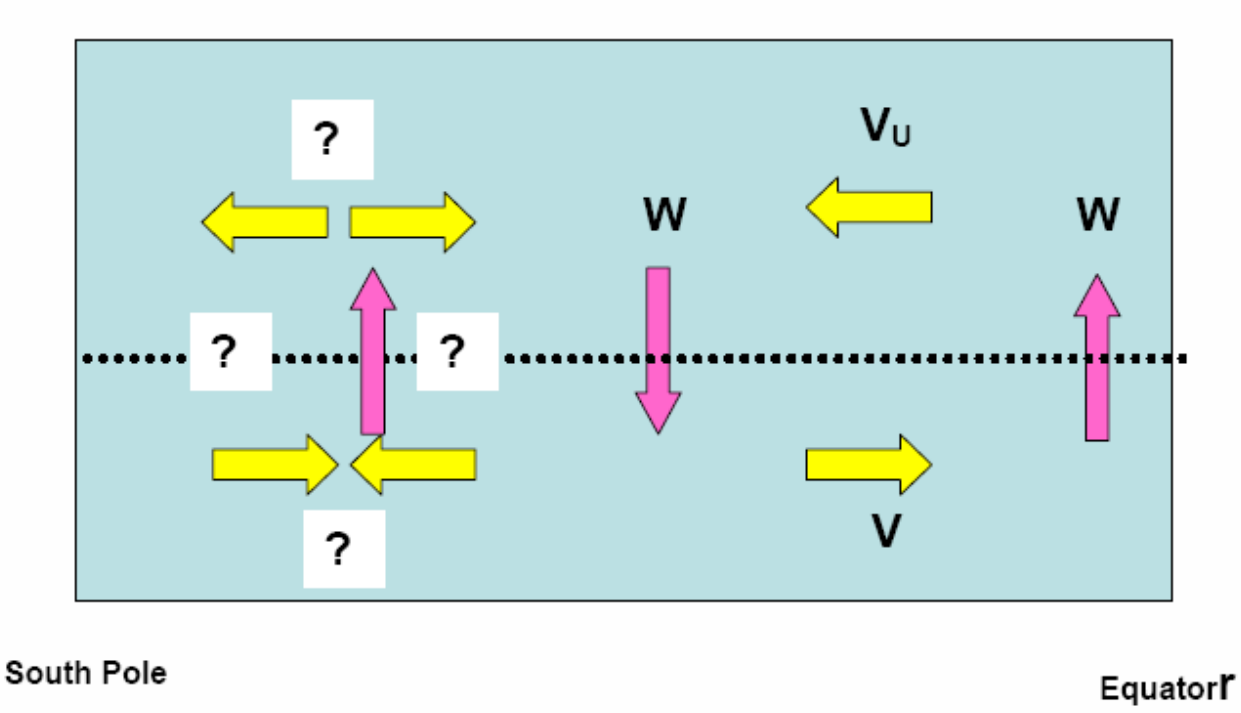

Fig. 7: *A simple 2-level representation of the zonally averaged circulation (Southern hemisphere).*

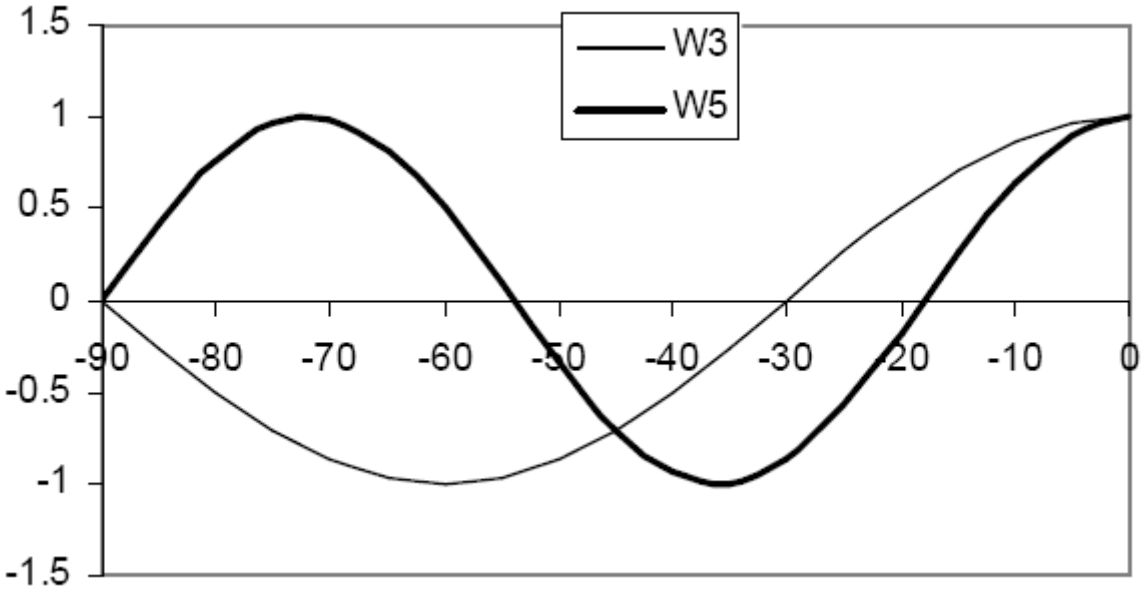

Fig. 8: *Simple solutions for W.*

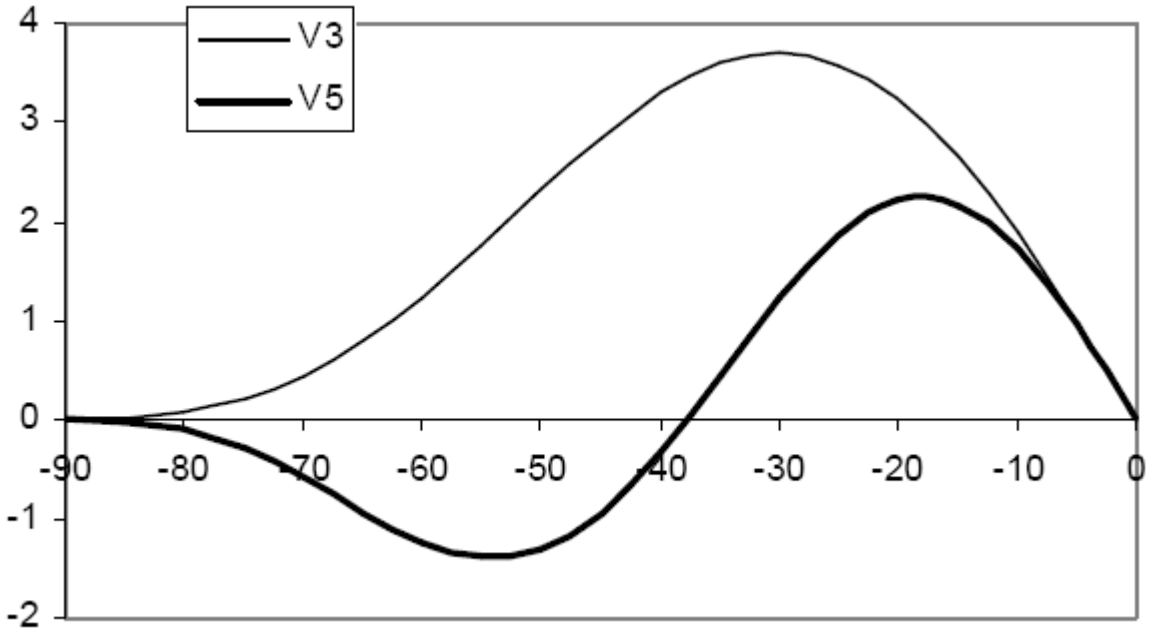

Fig. 9: *Simple solutions for V.*

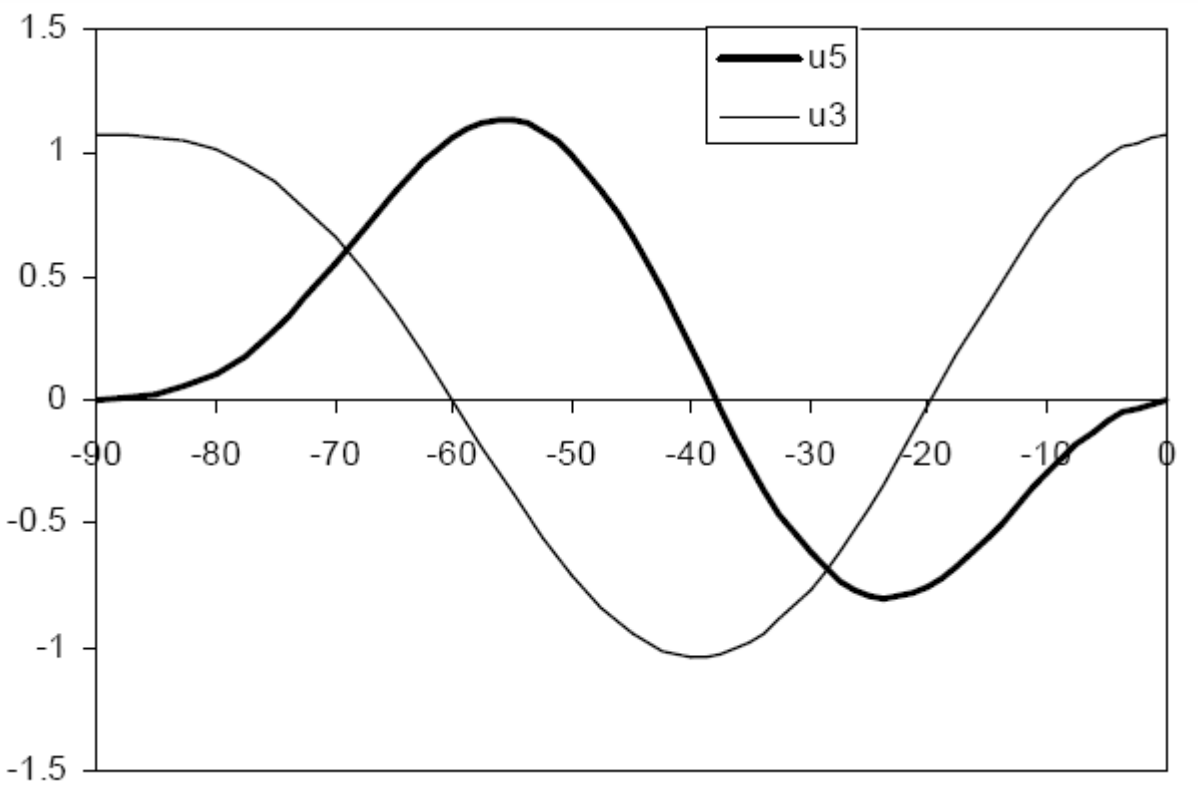

Fig. 10: *Simple solutions for the zonally averaged velocity U_3 and U_5 corresponding to (V_3, W_3) and (V_5, W_5).*

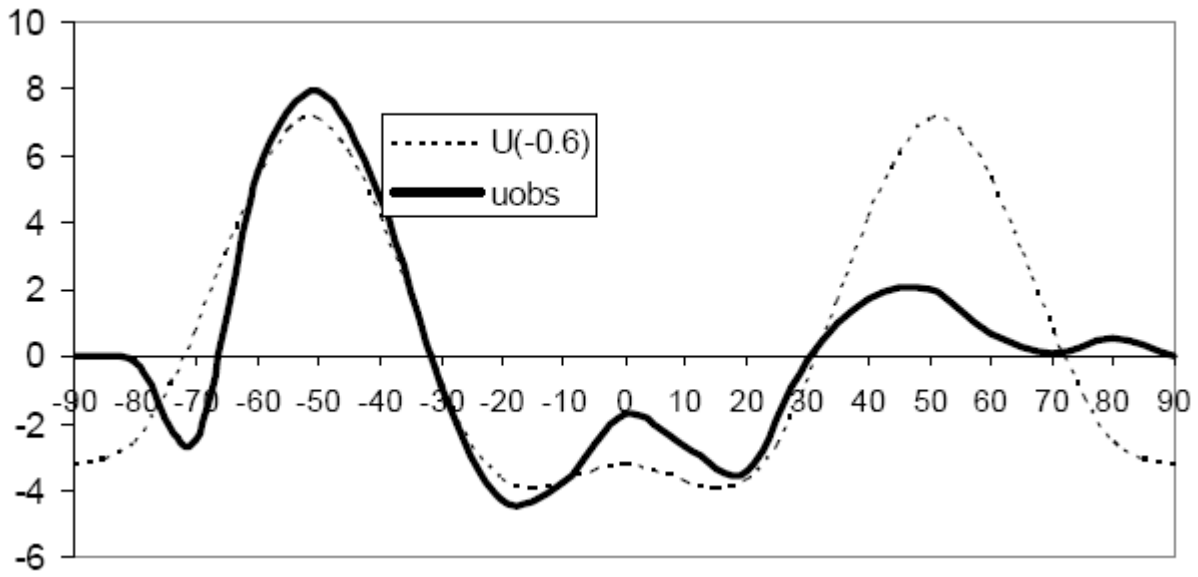

Fig. 11: *Comparison between observed U (1000 hPa) and U (-0.6) .*

Table 1: *Features of the solutions (in the Southern Hemisphere) for W, V and U when S varies from -0.8 to 0.0.*

Feature	Change	Implication	See:
W tropics	**+**	Wetter	Allan and Soden (2007)
Latitude of W=0	**-**	Widening of the tropics	Seidel et al. (2007)
W mid to high latitudes	**-**	Drier	Allan and Soden (2007)
V tropics	**+**	Stronger HC	Oort and Yienger (1996)
Latitude of V=0	**-**	More extensive HC	Lu et al. (2008)
V mid to high latitudes	**-**	Weaker FC	
Trade winds	**-**	Weaker Walker circulation	Oort and Yienger (1996) Vechi et al. (2006) Power and Smith (2007)
Westerlies	**-**	Slower moving storm tracks	
Latitude of U max	**-**	Poleward shift in storm tracks	
Polar easterlies	**- and change sign**	Weaken and become westerlies	

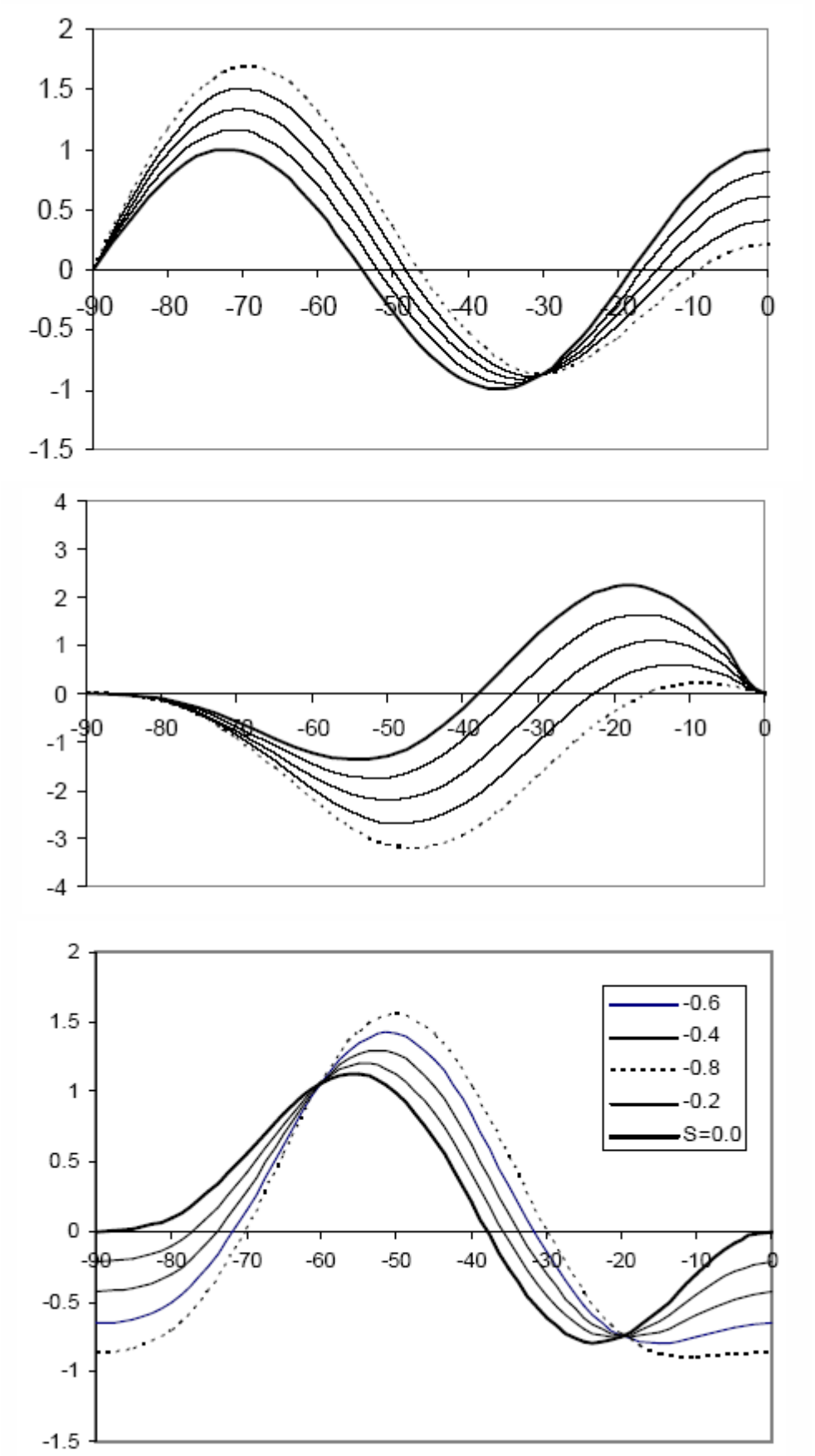

Fig. 12: *The effect of varying values of S on W (a), V (b) and U (c).*